

Figure 3 Injection and induced current waveform for 50 and 400 GHz SiC p^+n single-drift flat-profile IMPATT devices at 800 K when $V_{rf}/V_b = 0.5$

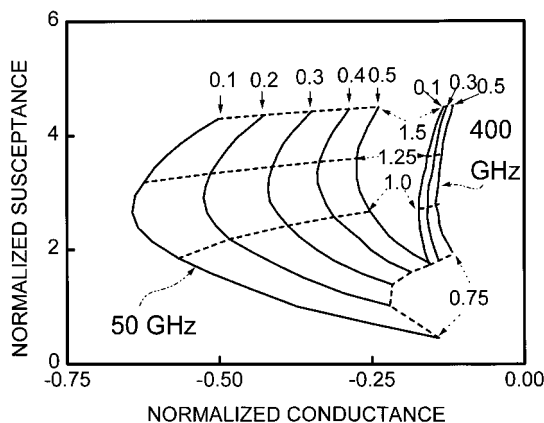


Figure 4 Normalized conductance and susceptance for 50 and 400 GHz SiC p^+n single-drift flat-profile IMPATT devices at 800 K. Solid arrows point to the normalized RF voltage amplitudes, and dashed arrows point to the normalized frequencies

The normalized injection current and the normalized induced current for 50 and 400 GHz SiC p^+n single-drift flat-profile IMPATT devices at 800 K 50% amplitude modulation are shown in Figure 3. The strong nonlinearity in the avalanche process leads to a sharper avalanche injection current pulse and a square-like induced current, while saturation of the ionization rates at higher electric fields results in a broadened avalanche injection current pulse and sinusoidal-like induced current as shown in Figure 3. Figure 4 illustrates the normalized admittance for 50 and 400 GHz SiC p^+n single-drift flat-profile IMPATT devices at 800 K. The larger conductance at low frequency comes from the strong nonlinearity in the avalanche process, while the susceptance mainly comes from the cold depletion capacitance. The decrease in quality factor at a lower frequency facilitates the impedance matching to the oscillator circuit, and the resulting device is less susceptible to series resistance.

DISCUSSION AND CONCLUSION

The simulation analyzed millimeter-wave SiC IMPATT oscillator devices at high temperature. A Read diode analysis is less accurate at the efficiency fall-off frequencies because there is no well-defined avalanche region at the frequencies where efficiency falls off. Thus, a full-scale simulation is

needed for better accuracy. Nonetheless, a Read-type analysis is sufficient to predict at what frequency the efficiency falls off. The efficiency remains high below 200 GHz frequency for a p^+n single-drift flat-profile structure. Thus, it is feasible to design a high-low or a low-high-low Read-type structure to further optimize the efficiency by reducing the voltage drop at the avalanche region. The output power and efficiency can be further improved by using a double-drift type design. In conclusion, millimeter-wave SiC IMPATT devices were analyzed at high temperature with temperature-dependent ionization rates and saturation velocity. Our simulation confirms the efficiency and power advantage of millimeter-wave SiC IMPATT oscillators.

ACKNOWLEDGMENT

This work was supported by the National Science Council of the Republic of China under Contract NSC 87-2213-E-005-019.

REFERENCES

1. M. Ruff, H. Mitlehner, and R. Helbig, "SiC Devices: Physics and Numerical Simulation," *IEEE Trans. Electron Devices*, Vol. 41, 1994, p. 1040.
2. C. Weitzel, J. W. Palmour, C. H. Carter, Jr., K. Moore, K. J. Nordquist, S. Allen, C. Thero, and M. Bhatnagar, "Silicon Carbide High-Power Devices," *IEEE Trans. Electron Devices*, vol. 43, 1996, p. 1732.
3. I. Mehdi, G. I. Haddad, and R. K. Mains, "Microwave and Millimeter-Wave Power Generation in Silicon Carbide Avalanche Devices," *J. Appl. Phys.*, Vol. 64, No. 3, 1988, p. 1533.
4. C. C. Meng and H. R. Fetterman, "A Theoretical Analysis of Millimeter-Wave GaAs/AlGaAs Multiquantum Well Transit Time Devices by the Lucky Drift Model," *Solid-State Electron.*, Vol. 36, 1993, p. 435.
5. T. Misawa, "High-Frequency Fall-Off of IMPATT Diode Efficiency," *Solid-State Electron.*, Vol. 15, 1972, p. 447.
6. S. M. Sze, *High-Speed Semiconductor Devices*, John Wiley & Sons, New York, 1990, p. 555.

© 1998 John Wiley & Sons, Inc.
CCC 0895-2477/98

MICROWAVE PROPERTIES OF $Sr_{0.5}Ba_{0.5}TiO_3$ THIN-FILM INTERDIGITATED CAPACITORS

S. W. Kirchoefer,¹ J. M. Pond,¹ A. C. Carter,¹ W. Chang,¹ K. K. Agarwal,^{1,*} J. S. Horwitz,¹ and D. B. Chrisey¹

¹ Naval Research Laboratory
Washington, District of Columbia 20375-5347

Received 19 December 1997

ABSTRACT: Interdigitated capacitors have been fabricated on ferroelectric thin films of $Sr_{0.5}Ba_{0.5}TiO_3$. These devices have been characterized at microwave frequencies from 50 MHz to 20 GHz, and have a 3.4:1 tuning range over a 1–40 V bias range. This is shown to originate from a relative dielectric constant tuning of 3.8:1. The microwave losses exhibited by these capacitors are comparable to those of commercially available semiconductor varactors for frequencies greater than 1 GHz, and should be useful for tunable microwave circuits in some 300 K

*Currently with Texas Instruments, Inc., Plano, Texas.

Key words: ferroelectric; varactor; interdigitated capacitor

INTRODUCTION

Ferroelectric materials have been long known to have unique dielectric properties. In principle, these properties can be employed to make tunable microwave devices and circuits [1–3]. Recent work utilizing pulsed-laser deposition to grow ferroelectric thin films has demonstrated improvements in thin-film material characteristics that hold promise for tunable microwave electronic components [4]. These deposition and processing refinements have resulted in ferroelectric thin films which retain a large dependence of the susceptibility on the applied electric field with acceptably low microwave losses for some applications. This paper reports results for interdigitated thin-film capacitors that have been fabricated on $\text{Sr}_{0.5}\text{Ba}_{0.5}\text{TiO}_3$. This composition results in a Curie temperature near 300 K, and films which exhibit large dielectric constant dependence on electric field.

DEVICE FABRICATION

The deposition technique used for the formation of these ferroelectric films has been described extensively in prior work [5–6]. A pulsed excimer laser is used to vaporize material from a high-density sintered target of compressed powder, containing the stoichiometric ratios necessary for the desired film. A (100) LaAlO_3 or MgO substrate is held with silver paint in proximity to the target on a stainless steel stage heated to 750°C. Material is deposited on the sample at a rate of 2 Å per laser pulse, to a desired thickness of 0.4 μm. The resulting film is single phase and (100) oriented. The film compositions and thicknesses are verified by Rutherford backscattering measurements [7].

An array of interdigitated capacitors is fabricated on these films by photolithography and metal lift-off patterning. In order to reduce metal losses at microwave frequencies, a 1.5 μm thick silver metallization is employed to define the interdigitated structure. The desired pattern is first developed as windows in a trilayer resist. The resist is composed of successive depositions of PMMA, a thin metal film, and Microposit 1818 photoresist. A mask with the desired pattern is used to expose and develop the 1818 resist. The pattern is transferred to the metal film by wet etching. The 1818 resist is removed by flood exposure and developing, and the sample is flood exposed by deep UV in order to transfer the pattern to the PMMA. After the PMMA is developed, the sample is ready for the final metallization. Silver is deposited over the sample, to a thickness of 1.5 μm, followed by a thin gold layer which preserves the surface for electrical contact. Lift-off in acetone is used to delineate the capacitor pattern. A variety of device geometries is fabricated. Finger length varies from 15 to 125 μm, and finger gap varies from 5 to 12 μm. The total number of fingers is any individual device varies from 8 to 12.

MEASUREMENTS

Measurements are made on these capacitors to determine their capacitance and device quality factor (Q). The devices are connected via 200 μm pitch Picoprobe microwave probe to an HP 8510C vector network analyzer, and microwave

**This article is a US Government work and, as such, is in the public domain in the United States of America.

reflection measurements (S_{11}) are performed. DC bias is applied to the capacitor under test through the internal bias tees of the network analyzer test set. The device bias is set initially at –40 V, and swept in 5 V steps to +40 V, and then back to –40 V. The 40 V limit is imposed on the experiment by the limitations of the bias tees of the network analyzer, and does not represent any inherent breakdown limitation of the devices. Data are collected at 401 frequency points in the range from 50 MHz to 20 GHz. The dc-bias network is capable of measuring low-frequency resistance and reactance, as well as supplying the needed bias voltages. Data on both the dc characteristics and microwave S_{11} measurements are collected for each bias point, and are stored in computer files for data reduction and analysis. The data are fitted to a parallel resistor–capacitor model to determine capacitance and Q .

A pair of S_{11} reflection data curves is shown in Figure 1. These data were taken at 0 and 40 V dc bias over the frequency range from 50 MHz to 20 GHz. As shown in Figure 2, the dimensions of this interdigitated capacitor are: finger overlap length = 80 μm, finger width = 5 μm and gap = 5 μm. The ferroelectric thin film is $\text{Sr}_{0.5}\text{Ba}_{0.5}\text{TiO}_3$ with a thickness of 0.4 μm on a 508 μm thick single-crystal LaAlO_3 substrate. The departure from expected capacitor-like response observed near the short-circuit point on the Smith chart occurs at frequencies approaching 20 GHz. This significant departure from discrete device behavior is a result of the wavelength in the dielectric approaching the dimensions of the device geometry due to the high relative dielectric constant of the ferroelectric thin film. As a result, the device is no longer electrically small at the upper end of the test frequency range, and thus, the lumped-element model employed is no longer applicable. To avoid introducing this error into the lumped-element models, data which exhibit such departure from discrete device behavior are not used, resulting in an upper frequency limit for the analysis of most devices occurring in the range from 5 to 15 GHz. Since the primary loss mechanism is expected to be due to the dielectric loss tangent of the ferroelectric, we have modeled the loss element as a parallel resistance. With devices such as this one that exhibit relatively low loss, the difference between values of capacitance and Q for a series resistor–capacitor

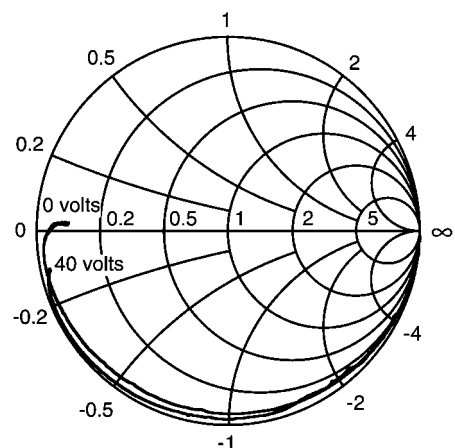


Figure 1 Plot of the reflection coefficient (S_{11}) on the Smith chart for a ferroelectric capacitor at 0 and 40 V bias over the frequency range from 0.05 to 20 GHz. The data span from the open-circuit point (∞) at low frequencies to near the short-circuit point (0) at high frequencies

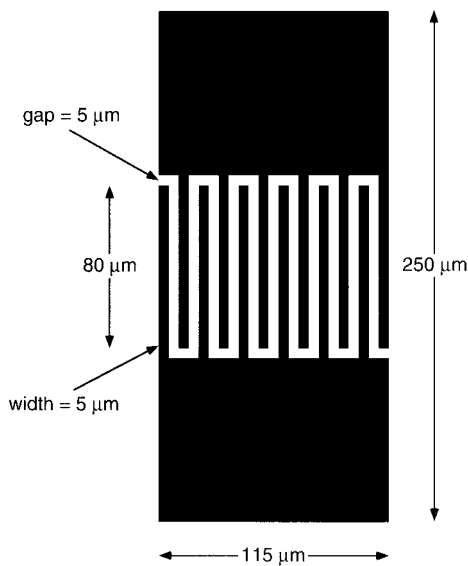


Figure 2 Interdigitated capacitor layout and dimensions

model versus a parallel resistor-capacitor model is not significant. For devices that have significant losses, a parallel network shows the best fit to those experimental data, and so we use a parallel model. If the metal film losses of the capacitor were dominant, one would expect a series resistance element to be necessary. Measurements of calibration devices fabricated on normal dielectric substrates have shown that the metal film resistance losses are negligible relative to the dielectric losses observed in the ferroelectric thin films, and so a series loss element is not normally needed in the model. Since the reflection measurements are all performed at low microwave power levels, the extracted device parameters are small signal in nature. Hysteresis is evident in some devices. However, for many microwave circuit applications which require a tunable reactance, the small-signal lumped-element model applied herein is sufficient as long as the losses are considered to be bias dependent.

Whereas microwave circuit design issued can be adequately addressed by parameterizing device capacitance and Q versus bias, quantifying the relative dielectric constant and loss tangent of the ferroelectric thin film is important in understanding and optimizing these materials for device applications. A pseudostatic model has been used successfully to determine the dielectric constant of the ferroelectric thin film from the measured interdigitated capacitor data [8].

RESULTS

The results of data analysis for the device of Figure 1 are shown in Figures 3 and 4. The capacitance curves displayed in Figure 3 are calculated from data taken in 2 GHz steps over the frequency range from 2 to 10 GHz. Figure 4 displays the curves for Q calculated from the same data set and over the same ranges as Figure 3. There is a systematic variation in capacitance and Q with frequency that is obvious from these families of curves. As expected, there is some residual hysteresis with bias voltage which can be seen if the bias is swept continuously back through the voltage range in the opposite direction. For the sake of clarity in Figures 3 and 4, the hysteresis is shown for 10 GHz only, but it is similar for all frequencies measured. The variation from the expected frequency-independent capacitance and Q can be shown to

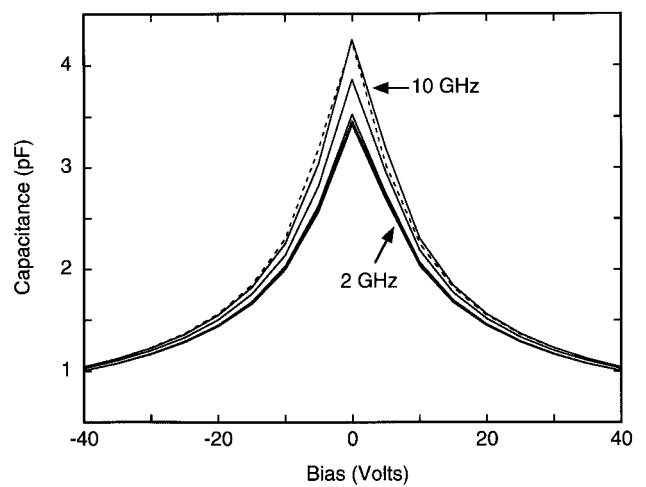


Figure 3 Capacitance versus bias voltage of a ferroelectric capacitor, changing monotonically with frequency for values of 2, 4, 6, 8, and 10 GHz. The data represent bias swept for -40 to 40 V, with the hysteresis present in the return sweep from 40 to -40 V shown as a dashed line for 10 GHz only

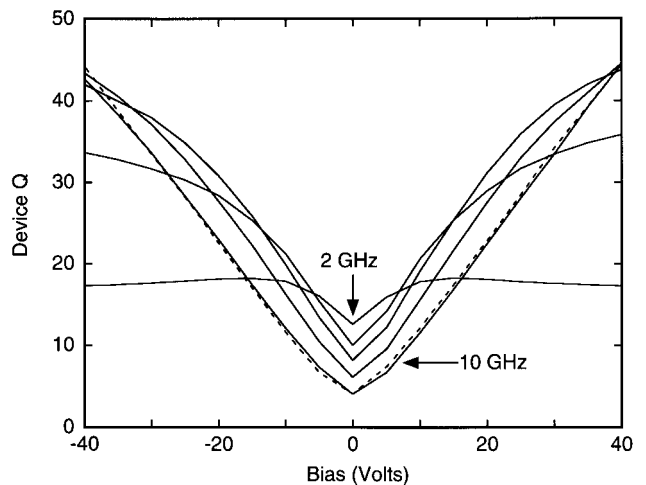


Figure 4 Device Q versus bias voltage of a ferroelectric capacitor, changing monotonically with frequency for values of 2, 4, 6, 8, and 10 GHz. The data represent bias swept for -40 to 40 V, with the hysteresis present in the return sweep from 40 to -40 V shown as a dashed line for 10 GHz only

originate in the data of Figure 1 which depart significantly from those of a discrete capacitor as the frequency increases. Additionally, the loss tangent of the ferroelectric is frequency dependent, which adds to the frequency dependence of the device Q . These departures from discrete device behavior are a result of the fact that the device can no longer be considered electrically small at the higher test frequencies.

Conformal-mapping-based models for interdigitated capacitors on layered substrates [8] have been applied to our device data. By definition, these models are only applicable at frequencies which are sufficiently low that the device is electrically small. Following [8], the relative dielectric constant of the ferroelectric thin film can be calculated given the geometry of the interdigitated capacitor, the thickness of the ferroelectric thin film, the thickness and dielectric constant of the substrate, and the measured capacitance. Figure 5 shows, for the measured data in Figure 1, the relative dielectric

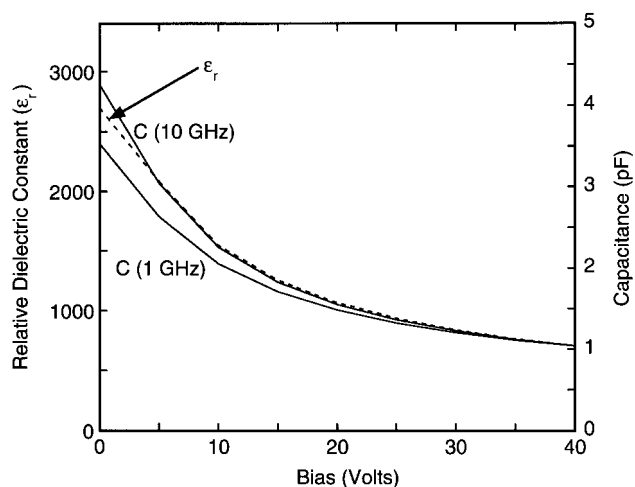


Figure 5 Relative dielectric constant and device capacitance at 1 and 10 GHz

constant of the ferroelectric thin film varying from 2700 at 0 V bias to 700 at 40 V bias. Although the conformal-mapping-based model is only valid when the device is electrically small, it is found that the values extracted from the measured capacitances vary by only $\pm 5\%$ up to 7 and 11 GHz at 0 and 40 V bias, respectively. Using the calculated 0 V ferroelectric relative dielectric constant, we note that the wavelength at 20 GHz in an infinite medium possessing a relative dielectric constant of 2700 in 290 μm . Since the finger overlap length is 80 μm , it is not surprising that the lumped-element approximation is not valid at the upper end of our measurements.

The measured device capacitance at 1 and 10 GHz is also plotted in Figure 5. There is a similarity between the calculated relative dielectric constant and the actual capacitance data. As can be seen from Figure 5, the relative dielectric constant tuning factor of 3.8:1 is slightly larger than the capacitance tuning range of 3.4:1. The fact that the tuning range of the capacitor is slightly less than that of the dielectric follows from the fixed capacitances, the substrate below, and the air above which, in parallel with the ferroelectric thin film, constitute the total device capacitance. In this case, these fixed parallel capacitances contribute 0.7 pF of the total device capacitance. The apparently larger tuning range at 10 GHz is a result of the interdigitated structure no longer being electrically small. The discrepancy is most pronounced at low applied electric fields, where the dielectric constant is the largest. Since the deviation from the simple capacitance behavior always occurs near the short-circuit point on the Smith chart, it is not a cause for concern for most microwave applications. There is little utility for operating varactors with impedance values that are so close to an apparent short circuit. Most applications require capacitors which are designed to operate in the regime where these capacitors can be regarded as electrically small devices. Either scaling down the designed capacitance or operating at a lower frequency will minimize the size-related effects and result in useful devices. The anomalous behavior seen at high frequencies does not present a serious limitation for practical application of this technology.

CONCLUSIONS

In conclusion, we have fabricated varactors from ferroelectric thin films that demonstrate considerably improved character-

istics over previous devices. For frequencies in excess of 10 GHz, these results are comparable to what is achieved by other conventional varactor technologies. Deviations from ideal discrete capacitor behavior have been shown to be a direct result of the extremely high dielectric constants associated with these materials.

ACKNOWLEDGMENTS

The authors wish to acknowledge the technical assistance of W. W. Moore and the helpful discussions of L. S. Knauss and C. Rauscher. This work has been funded by the Office of Naval Research.

REFERENCES

1. V. K. Varadan, D. K. Gohdgaonkar, V. V. Varadan, J. F. Kelly, and P. Glikerdas, "Ceramic Phase Shifters for Electronically Steerable Antenna Systems," *Microwave J.*, Vol. 35, Jan. 1992, pp. 116-127.
2. V. Chivukula, J. Iowski, I. Emesh, D. McDonald, P. Leung, and M. Sayer, "Dielectric Properties of Ferroelectric Thin Films in the Frequency Range of mHz-GHz," *Integr. Ferroelectr.*, Vol. 10, No. 1-4, 1996, pp. 247-255.
3. A. Outzourhit, J. U. Trefny, T. Kito, B. Yarar, A. Nazirpour, and A. M. Hermann, "Fabrication and Characterization of $\text{Ba}_{1-x}\text{Sr}_x\text{TiO}_3$ Tunable Thin Film Capacitors," *Thin Solid Films*, Vol. 259, Apr. 15, 1995, pp. 218-224.
4. J. S. Horwitz, D. B. Chrisey, J. M. Pond, R. C. Y. Auyeung, C. M. Cotell, K. S. Grabowski, P. C. Dorsey, and M. S. Kluskens, " $\text{Sr}_x\text{Ba}_{1-x}\text{TiO}_3$ Thin Films for Active Microwave Device Applications," *Integr. Ferroelectr.*, Vol. 8, No. 1-2, 1995, pp. 53-64.
5. K. S. Graowski, J. S. Horwitz, and D. B. Chrisey, "Pulsed Laser Deposition of Oriented $\text{PbZr}_{0.54}\text{Ti}_{0.45}\text{O}_3$," *Ferroelectrics*, Vol. 116, No. 1-2, 1991, pp. 19-33.
6. J. S. Horwitz, D. B. Chrisey, K. S. Grabowski, and P. E. Leuchtner, "Pulsed Laser Deposition of Electronic Ceramics," *Surf. Coat. Technol.*, Vol. 51, Apr. 15, 1992, pp. 290-298.
7. L. A. Knauss, J. S. Horwitz, D. B. Chrisey, J. M. Pond, K. S. Grabowski, S. B. Qadri, E. P. Donovan, and C. H. Mueller, "Dielectric Susceptibility and Strain in $\text{Sr}_{1-x}\text{Ba}_x\text{TiO}_3$ Ferroelectric Thin Films Grown by Pulsed Laser Deposition," *Mater. Res. Soc. Symp. Proc.* Vol. 388, Apr. 1995, pp. 73-78.
8. S. S. Gevorgian, T. Martinsson, P. I. J. Linner, and E. L. Kollberg, "CAD Models for Multilayered Substrate Interdigital Capacitors," *IEEE Trans. Microwave Theory Tech.*, Vol. 44, June 1996, pp. 896-904.

© 1998 John Wiley & Sons, Inc.
CCC 0895-2477/98

PLANE WAVE PROPAGATION THROUGH A UNIAXIAL CHIRAL SLAB AND TRANSMISSION COEFFICIENT

Savaş Uçkun¹

¹ Department of Electrical and Electronics Engineering
University of Gaziantep
27310 Gaziantep, Turkey

Received 31 October 1997; revised 27 January 1998

ABSTRACT: Plane wave reflection and transmission from a uniaxial chiral interface have recently been found. In this letter, the propagation of the electromagnetic waves through an infinite slab of a lossless uniaxial chiral medium is formulated for normal incidence, and an equation for the total transmission dyadic coefficient is derived. © 1998 John Wiley & Sons, Inc. *Microwave Opt Technol Lett* 18: 171-174, 1998.